

## Silicon heterojunction solar cells: Excellent candidate for low light illuminations



Rupendra Kumar Sharma <sup>a,\*</sup>, Abhinav Deep Pakki <sup>a</sup>, Jakub Holovský <sup>a,b</sup>

<sup>a</sup> Centre for Advanced Photovoltaics, Faculty of Electrical Engineering, CTU in Prague, Technická 2, 166 27, Prague, Czech Republic

<sup>b</sup> Institute of Physics, Czech Academy of Sciences, Cukrovarnická 10, 162 00, Prague, Czech Republic

### ARTICLE INFO

**Keywords:**  
 Solar cells  
 Silicon hetero-junctions  
 Intensity dependence  
 Low illumination  
 TCAD simulation

### ABSTRACT

The current solar cells and modules are marketed according to the behaviour at standard test conditions (STC), however, these devices are more often operated at lower irradiance levels. The dependence on illumination stems mainly from the voltage at the open circuit and at the maximum power point. The latter might also be strongly influenced by serial resistance, but that is more an engineering problem not addressed here. More fundamentally, the voltage is determined by quasi-Fermi levels at the contacts. In the case of unconstrained conductivity between the absorber and electrode, the quasi-Fermi levels are flat, and determined by their splitting in the absorber. Our analysis shows that the modulation doping mechanism working in Si heterojunction solar cell between the doped amorphous Si layer with a higher bandgap and crystalline absorber with a lower bandgap can, for certain parameter settings, lead to strongly depleted contact layer that limits conduction. This is a prerequisite for decoupling the quasi-Fermi level between contact and absorber and offers the possibility for additional voltage increase. Based on this understanding, we simulate a heterojunction solar cell with a varying thickness and doping of amorphous silicon p-type contact. We demonstrate that for a certain combination of thinner or lower-doped contact, higher efficiency at low illumination can be achieved compared to the technological baseline. This is fully in line with the experimental findings. This analysis is crucial not only for using solar cells for indoor applications but also for designing photovoltaic modules optimized for low irradiance, potentially increasing the level of self-sufficiency of buildings.

### 1. Introduction

The solar cell efficiency and power rating for PV modules are reported at the standard test conditions (STC) implying 1 sun illumination ( $1000\text{W/m}^2$ ) [1], however, the PV modules rarely experience 1 sun illumination. Depending on the location, the annual energy yield of the PV systems may strongly depend on the low illumination characteristics of solar cells [2–5]. Advanced crystalline silicon (c-Si) solar cells [6,7] have demonstrated superior performance at STC i.e., a world record conversion efficiency of 26.81 % and fill factor (FF) of up to 86.59 % has been achieved recently by the LONGi team [8]. Nevertheless, these cells might had issues due to the low parallel resistance under low illumination conditions [9]. In contrast, the advantage of low irradiance used to be the domain of thin-film solar cells, including hydrogenated amorphous silicon (a-Si:H) [10,11], copper-indium-gallium-selenium [12], cadmium telluride [13,14], gallium arsenide [15], and organic solar cells [16,17]. Later, when parallel resistance had not been an issue

anymore, c-Si technology focused on lowering serial resistance by increasing the number of busbars and eventually by cutting the cells in half to boost the performance at STC [18,19]. As a result, the performance of c-Si devices at any irradiance level is almost free from the effects of parasitic resistance. Irradiance dependence is thus solely the effect of semiconductor structure, where various technological factors play role and makes the understanding much more complex.

Recently, an experimental study focused on the thickness of the c-Si absorber showed that thinner wafers give slightly better efficiency at low light intensity [20]. Silicon heterojunction (SHJ) solar cells with n-doped amorphous silicon carbide layer with varying carbon contents displayed both improved temperature coefficient and higher relative efficiency at low-illumination [21]. In our previous work, we investigated the requirement on thickness and doping and its relaxation under lower irradiance [22]. We derived an analytical expression, called contact strength [23] that was mainly addressing the extracted voltage. That approach suggested that under low irradiance, requirements for

\* Corresponding author.

E-mail address: [sharmrup@fel.cvut.cz](mailto:sharmrup@fel.cvut.cz) (R.K. Sharma).

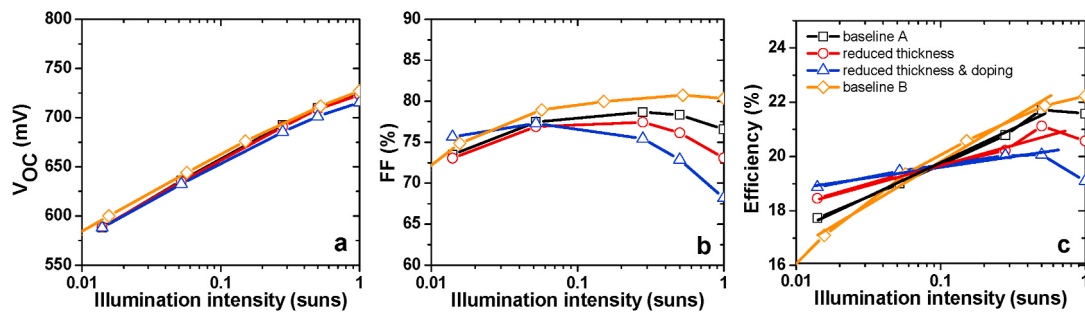


**Fig. 1.** The experimental results (a)  $V_{OC}$  (b) FF (c) Efficiency for baseline A, reduced thickness, reduced thickness & doping, and baseline B, plotted for a wide range of illumination (0.1–1.0 Suns).

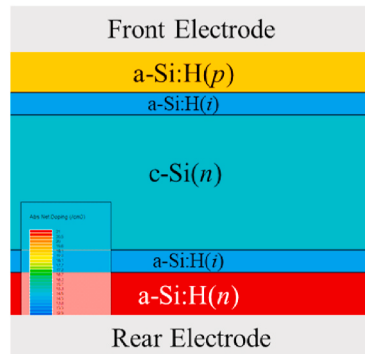


**Fig. 2.** The simulated structure of SHJ solar cell realized in TCAD device simulator, the colour bars corresponding to the doping level in various layers of SHJ solar cell (the layer thicknesses are not to scale).

contact materials relaxed so that alternative (e.g., lower absorbing) layers could be used while maintaining (or even slightly improving due to reduced absorptance) the low irradiance behaviour. To that end, any potential improvement was explained only as an optical effect. In this work, we address the effect of purely electrical increase in low light efficiency.

The subject of the current study is the technology of silicon heterojunction (SHJ) solar cell. In the experimental part, two different generations of SHJ solar cells optimized for STC (baseline process) are compared also with cells prepared with intentionally thinner and lower-doped p-layers. For the technological details, refer to our previous publications [22,23]. The core part of this paper and the main approach is the simulation in semiconductor equation solver ATLAS Silvaco with varying of p-layer doping, its thickness, front electrode work function (WF), and the contact defect density. The aim is to reproduce and explain the effect of efficiency improvement at the low illumination level that was experimentally observed. The understanding of the effects

first requires accepting the fact, that the Quasi Fermi Level Splitting (QFLS) in the absorber is not a universal limiting factor for voltage, and it can be manipulated by electric field inside low-conductive layer at the contact. While introducing the concept of contact strength is following the rule “the stronger the better”, in this paper we consider the competing effect between contact strength and additional electric field build-up over low-conductive contact, where this simple rule may not be valid.

## 2. Reproducing experiment by computer simulation

The experimental results for the baseline device A [22], device with reduced thickness, with reduced thickness & doping together, and the device baseline B [23] is shown in Fig. 1. The different trends in efficiency versus illumination intensity are worth noticing.

Under low illumination (<0.1 suns), cells with reduced thickness and both reduced thickness and doping result in an improvement of efficiency with sacrificing the efficiency at higher intensities compared to baseline A. Baseline device B is even more optimized for higher efficiency at STC, so that the difference is even larger. As we can see from illumination dependence of open circuit voltage ( $V_{oc}$ ) in Fig. 1a) the voltage behavior as well as the ideality factor (that would produce different slope of  $V_{oc}$  intensity dependence), is not the source of this behavior. Instead, it is the fill factor (FF) shown in Fig. 1b). Note that even though the contact strengths are different, the efficiencies around 0.1 sun are very similar, meaning that photogenerated currents are also different, pointing to the effect of different contact transparency. This can produce differences of a few percent relatively, but not that we see in Fig. 1c) at 0.01 sun.

The device was replicated in Silvaco semiconductor device simulator (Fig. 2). Electrode here means either a metal or degenerated semiconductor such as ITO. The contact on the rear side is idealized for electrons and unchanged for all the simulations performed. The parameters changed are the a-Si:H (*p*) contact layer thickness ( $t_{cont}$ ), doping ( $N_{cont}$ ) and defects density ( $D_{cont}$ ) which is crucial for hole

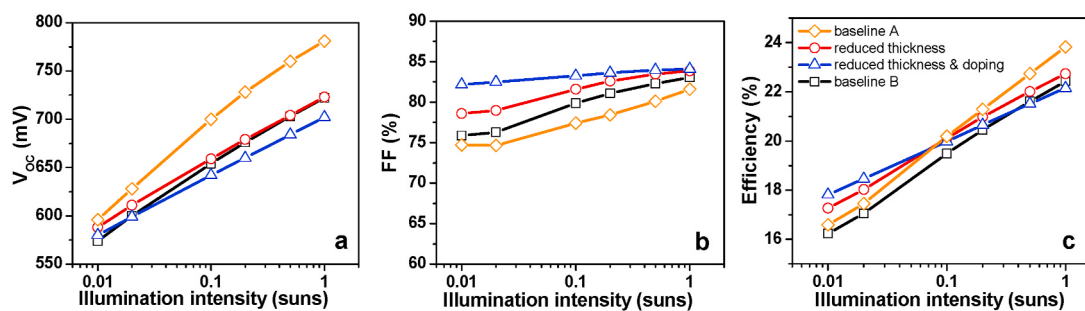


**Fig. 3.** TCAD simulation results (a)  $V_{OC}$  (b) FF (c) Efficiency are plotted for a wide range of illumination (0.1–1.0 Suns). (i) baseline A: 10 nm thick a-Si:H(*p*) layer doped with  $1.5 \times 10^{19} \text{ cm}^{-3}$ , (ii) reduced thickness: 5 nm thick a-Si:H(*p*) layer doped with  $1.5 \times 10^{19} \text{ cm}^{-3}$ , (iii) reduced thickness & doping: 5 nm thick a-Si:H(*p*) layer doped with  $1.0 \times 10^{19} \text{ cm}^{-3}$ , (iv) baseline B: 10 nm thick a-Si:H(*p*) layer doped with  $1.0 \times 10^{19} \text{ cm}^{-3}$ .

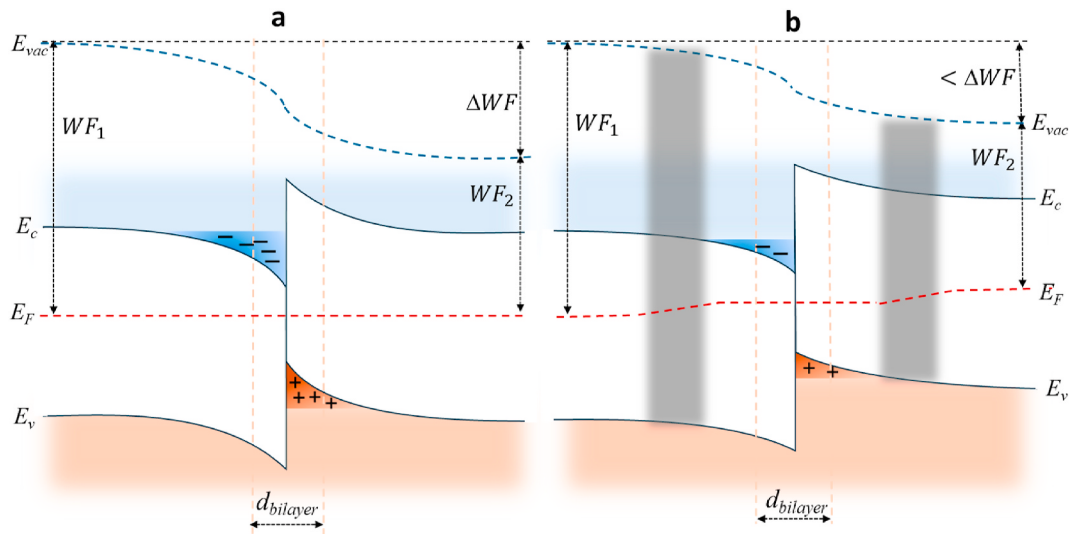


**Fig. 4.** Junction of materials with different work function. a) represent usual case and b) represents the case when there is not enough available charge, and the nearby regions are depleted and become almost insulating allowing electric field build-up (Fermi level gradient) and eventual potential balance.

selective SHJ solar cell performance [24]. One-dimensional (1-D) simulations were carried out because the lateral path is not contributing to the current flow [25]. The details of the simulation models and calibrated parameters are provided in our recently published article [23].

The trend in experimental results is reproduced by computer simulations (Fig. 3) and it is confirmed that FF plays a crucial role in improving the cell performance at lower illumination. The difference in FF between experimental (Fig. 1b) and simulation (Fig. 3b) at higher illumination may be caused by various resistances in real SHJ solar cell. Nevertheless, the deviations of FF intensity dependence from almost straight lines are similar for different cases and are not impacting the crossover at  $< 0.1$  suns. Our goal is to investigate other effects than resistance, so in the simulations the resistances were deliberately kept low. We study this behaviour in more details in Results section.

### 2.1. Understanding cell operation at low illuminations

The effective carrier extraction requires sufficiently non-uniform concentration of electrons and holes (produced by combination of many involved forces) that must be maintained in the absorber, especially for illuminated case. The non-uniform distribution of electrons and holes must prevent equilibration of these carriers over the bandgap – recombination. This nonuniformity can be realized mainly by enough band bending. The overall band bending is dictated by two rules: i) Vacuum level is continuous. ii) For the regions that are in thermodynamic equilibrium, Fermi level must be flat. The flatness of (quasi-)Fermi level is perturbed when there is not enough carrier flow to provide the equilibration, which can happen in two cases; either the

band diagram contains too high barrier [23] or the number of carriers between the two region is very low (depletion). The latter case is important for low irradiance.

According to these two rules, we conclude that overall bend bending (including the contributions in contacts) is summing up to work function difference, or there must be the case of restricted carrier flow. Band bending in the absorber can be further produced by charge in contacts. In the contact strength equation [23], the work function and charge are both in linear terms, suggesting that band bending scales with charge. Indeed, if we sketch the junction of two materials with work function difference  $\Delta WF$ , see Fig. 4a) the charges are stored in the narrow charge bilayer of given thickness labelled  $d_{bilayer}$  that resembles a capacitor and capacitor voltage scales with the stored charge. Should the  $\Delta WF$  be equal to band bending the (capacitor) charge must be provided by the material itself and as we often deal with the situation of thin layers, the charge might not be enough, causing depletion of surrounding regions, see Fig. 4b). Note that in our nomenclature the depleted region is the one that has no free carriers. Junction is on the other hand full of carriers.

According to rule ii), Fermi level is flat at the junction, but in the depleted regions, due to the fact, that the region is almost insulating, the electric field can exist, and Fermi level can be tilted (Fig. 4b). This effect is interesting, as it can produce Fermi level that is not flat while still representing equilibrium case of material in electrical contact. Obviously, due to the low conductivity, this can only work for low current, as in the cases of low irradiances.

In the actual heterojunction, this effect of depleting one part of semiconductor is even stronger due to the tendency of carriers to move from high bandgap to low bandgap region. As a result, the carrier

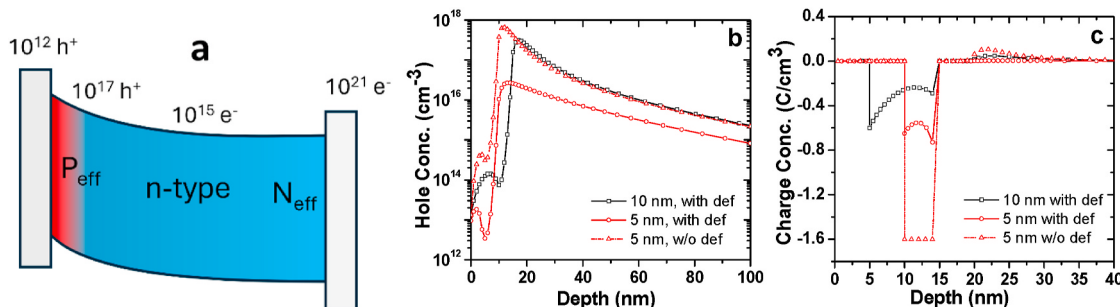


**Fig. 5.** a) the spatial redistribution of electron and hole densities, b) accurate simulation for 10 nm and 5 nm cases at 0.01 sun, and c) the net charge of the contact resulting from the density redistribution.

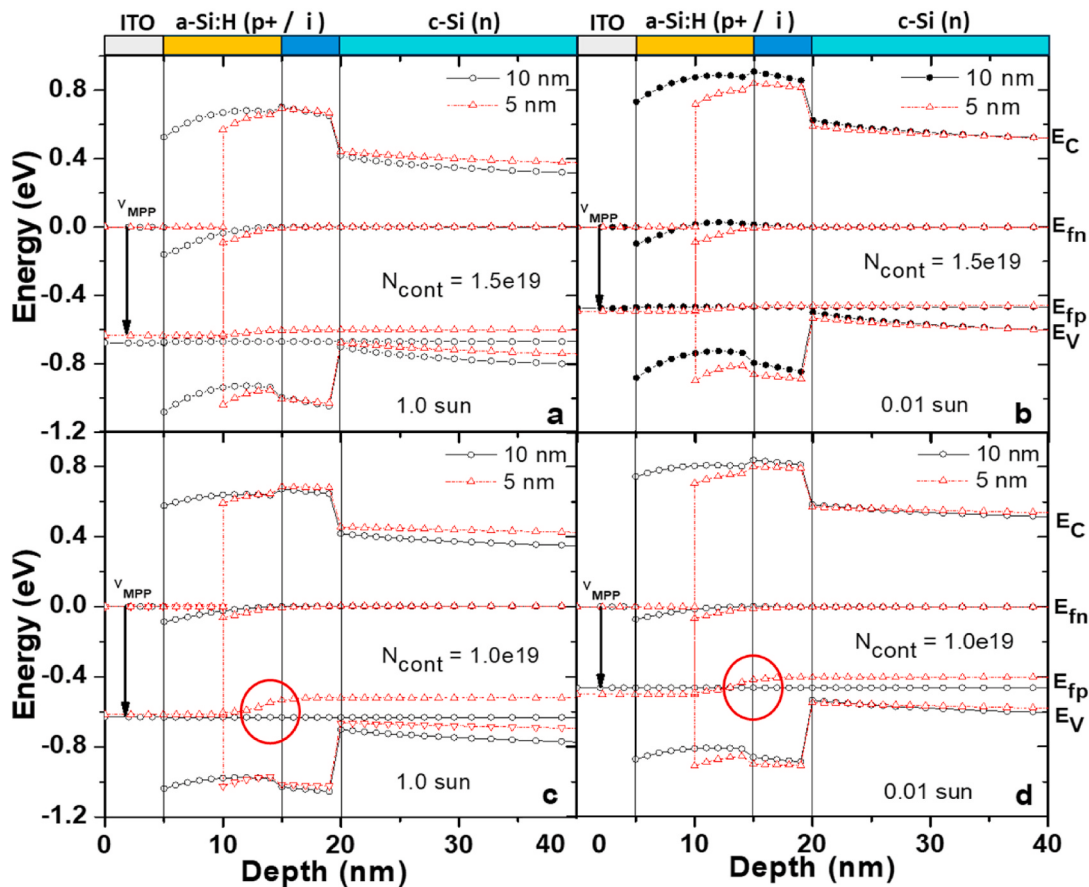


**Fig. 6.** Energy band diagram at MPP for the contact layer thickness of 10 nm and 5 nm (a)  $1.5 \times 10^{19} \text{ cm}^{-3}$ , 1.0 sun (b)  $1.5 \times 10^{19} \text{ cm}^{-3}$ , 0.01 suns (c)  $1.0 \times 10^{19} \text{ cm}^{-3}$ , 1.0 sun (d)  $1.0 \times 10^{19} \text{ cm}^{-3}$ , 0.01 suns. For the latter two cases the gradient of hole quasi-Fermi level happens if the layer is only 5 nm thick – indicated by circles.

concentration is entirely different from their original technological values (Fig. 5a). This effect is called modulation doping. The actual simulated concentration of holes in Fig. 5b shows that the highest concentration is 10 nm apart from the electrode, while in the contact itself (the first 10 nm) is completely depleted. Fig. 5c shows the net total (negative) charging, that is huge in the contact, similarly as in the inversion layer type solar cell [26] where the band bending is produced by charged layer instead of doped layer.

In Fig. 5c, we observe that the effect of thickness and defects is fully in line with the concept of contact strength i.e., the total charge is provided by product of doping times thickness. Additionally, we make correction to defects, showing that defect states absorb large portion of charge, considerably reducing the charge availability. Contact strength can be therefore written as follows (symbol \* labelling the defect

correction):

$$\text{Contact Strength}^* = A_2 \cdot WF_{elec} + N_{cont} t_{cont} - D_{cont}^{\text{charged}} \quad (1)$$

In the next step, we analyse the simulated band diagrams at maximum power point (MPP) at 1.0 sun and 0.01 suns for 10 nm and 5 nm, a-Si:H(p) doped with  $1.5 \times 10^{19} \text{ cm}^{-3}$ , and  $1.0 \times 10^{19} \text{ cm}^{-3}$  (Fig. 6). For weaker contacts (5 nm doped with  $1.0 \times 10^{19} \text{ cm}^{-3}$ ), band bending in dark (not shown here) is smaller than stronger contact (10 nm doped with  $1.5 \times 10^{19} \text{ cm}^{-3}$ ). Since the low illumination leads to smaller quasi-Fermi level splitting, the weak contact strength is sufficient.

The case of low irradiance is shown in Fig. 6 b), d) and the case of doping in the a-Si:H(p) layer is shown in Fig. 6 c), d). In each panel, the case of lower thickness is shown. We can clearly identify the gradient in the hole quasi-Fermi level  $E_{fp}$  in all the cases of weaker contacts. (The

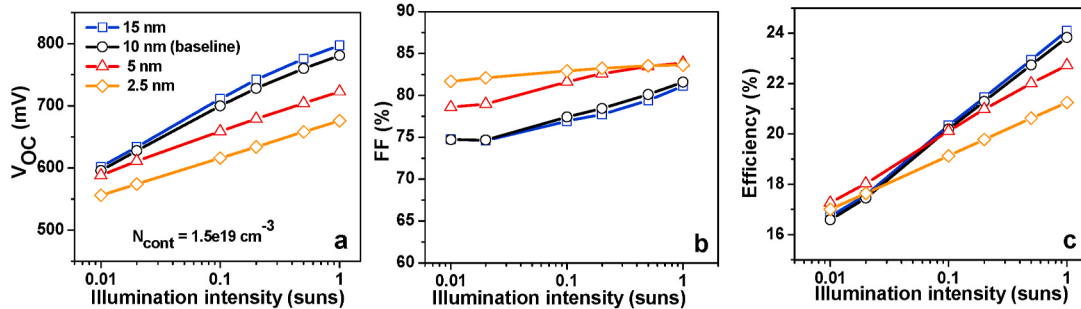


**Fig. 7.** The impact of variations of contact layer thickness ( $t_{cont}$ ) on simulated (a)  $V_{oc}$  (b) FF (c) Efficiency is plotted for a wide range of illumination (0.1–1.0 Suns). The p layer doping and front electrode WF is fixed to  $1.5 \times 10^{19} \text{ cm}^{-3}$  and 5.1 eV respectively.

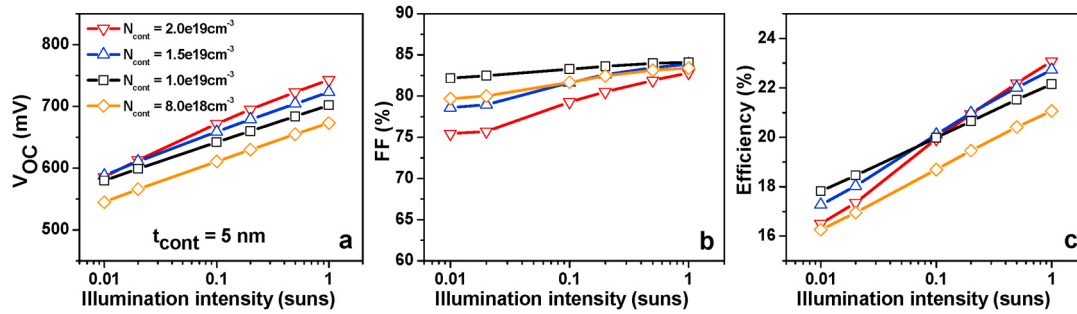


**Fig. 8.** The effect of variations of contact layer doping ( $N_{cont}$ ) on simulated (a)  $V_{OC}$  (b) FF (c) Efficiency for the case of p-layer thickness 5 nm, and front electrode WF 5.1 eV.

gradient in the quasi-Fermi level of minority carriers is not relevant). For 0.01 sun, this effect is producing considerable improvement in  $V_{MPP}$  (Fig. 6 b), d), however at 1 sun illumination, the effect of  $E_F$  gradient cannot compensate smaller quasi-Fermi level splitting in the absorber. The quasi-Fermi level positions in the absorber are determined by photogeneration but can be pushed towards the band edge by the doping, thus, the modulation doping form p-layer can enhance the quasi-Fermi level splitting on the p-type side of the solar cell. As the quasi-Fermi level for carriers in equilibrium must be flat, therefore the quasi-Fermi level splitting is enhanced in the whole structure. Note that the a-Si:H(p) layer is 5 orders of magnitude thinner than the absorber but also 5 orders of magnitude more doped.

Altogether, the modulation doping has two effects. If the doping is strong, it enhances the band bending and quasi-Fermi level splitting in the absorber. For weak doping, on the other hand, the p-layer become depleted and quasi-Fermi level can have a gradient. Both the mechanisms are enhancing  $V_{MPP}$ . The latter case is principally more advantageous, since smaller quasi-Fermi level splitting slows down recombination within the absorber. In contrast, depleted p-layer is not supporting higher irradiances and higher currents.

### 3. Results

Having explained the underlying effect of the increase in efficiency at low irradiance, we perform simulations more systematic. As a first step, we examine the impact of  $t_{cont}$  on cell performance in terms of  $V_{OC}$ , FF, and efficiency. The front electrode WF is set to 5.1 eV,  $N_{cont}$  to  $1.5 \times 10^{19} \text{ cm}^{-3}$  and  $t_{cont}$  is varied from 15 nm to 2.5 nm and compare it to baseline value of 10 nm (Fig. 7). The behaviour of  $V_{OC}$  well corresponds to our previously published metric called contact strength [23]. The concept is mainly based on extracted voltage determined by quasi-Fermi level splitting in the absorber and barrier height for carriers if any. Once the actual value of contact strength is above the required value for given quasi-Fermi level splitting, no significant increase in the efficiency is observed as in the case of 15 nm (compared to 10 nm). On the other hand, reducing  $t_{cont}$  reduces the capability to produce band bending in

absorber, essential for performance at higher illumination. For low illumination, thickness 5 nm still fulfils the requirements (Fig. 7a). The new and striking behaviour is observed in the fill factor (Fig. 7b). In low irradiance region, the reduction of  $t_{cont}$  from 10 nm to 5 nm (see also Fig. 7c) produces higher efficiency.

In further investigation, we stick to reduced thickness (5 nm) and vary the  $N_{cont}$  (Fig. 8). We lose at high illumination relatively (4 %) mainly due to  $V_{OC}$ , nevertheless at low irradiance, we can enhance the cell efficiency not only relatively (8 %), but also absolutely (1.5 %) for reduced doping ( $1.0 \times 10^{19} \text{ cm}^{-3}$ ) case, see Fig. 8c. The further reduction of  $N_{cont}$  to  $8.0 \times 10^{18} \text{ cm}^{-3}$  results in degrading cell performance overall because too weak contacts are not able to produce sufficient band bending.

The simulation results for FF at higher doping and at higher illumination (Fig. 3b) differ from the experimental data (Fig. 1b) because in real cells, there are several resistances, which reduces the FF at higher illumination. We extended our simulation to higher illumination (10 suns), so that the impact of series resistance will be noticeable. Note that at higher illumination, the FF drops for reduced thickness and doping case in comparison to higher doping: baseline A (Fig. 9a), like in the case of experimental data (Fig. 1b).

For readers' curiosity and following the current industrial trend reducing the requirement on front transparent contact conductivity which prefers a back p-contact junction, we performed a simulation with a p-contact layer on the backside. We observed a similar trend in our simulation with the p-contact layer on the frontside (Compare Fig. 9b and c). Moreover, a bit lower efficiency is observed in the case of p-type contact on the backside because of the low diffusion constant of holes compared to their counterpart electrons.

Simulated I-V curves for baseline, reduced thickness and both reduced thickness and doping is plotted in Fig. 10. We can further underline that improvement in FF is a key factor for enhancing efficiency at low illumination in comparison to the technological baseline.

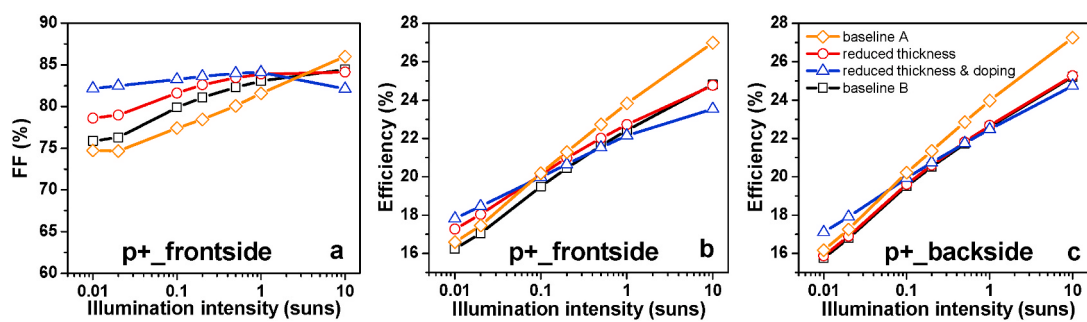


**Fig. 9.** (a) Fill Factor extracted from simulation for p + contact layer on the frontside (b) cell efficiency for p + contact layer on the frontside (c) cell efficiency for p + contact layer on the backside.

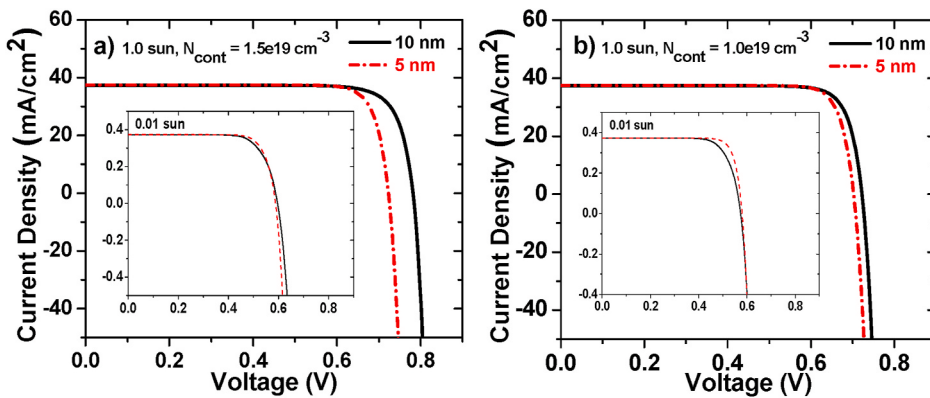


**Fig. 10.** Simulated IV curves for the contact layer thickness of 10 nm and 5 nm at different illuminations and contact layer doping **(a)**  $1.5 \times 10^{19} \text{ cm}^{-3}$  **(b)**  $1.0 \times 10^{19} \text{ cm}^{-3}$ , (Insets) IV curves at 0.01 suns.

#### 4. Conclusions

The experimental results demonstrate that thin and low-doped a-Si:H (*p*) contact can considerably improve cell efficiency under low light illumination while reducing efficiency at higher intensities. These results were reproduced by simulating the structure in the Silvaco device simulator. We have further optimized cell structure and demonstrate that through careful optimization of contact layer parameters (thickness and doping), we can improve cell efficiency at low illumination by almost 8 % while losing only about 4 % at 1 sun illumination, thus potentially increasing the total energy yield in cloudy countries. The underlying effect is related to the mechanism of modulation doping of absorber by a doped layer with higher bandgap, that is characteristic of silicon heterojunction technology. This is an important feature of this technology which is one of the potential candidates for future mainstream.

#### CRediT authorship contribution statement

**Rupendra Kumar Sharma:** Writing – original draft, Validation, Investigation, Formal analysis, Data curation. **Abhinav Deep Pakki:** Visualization. **Jakub Holovský:** Writing – review & editing, Supervision.

#### Declaration of competing interest

The authors declare that they have no known competing financial interests or personal relationships that could have appeared to influence the work reported in this paper.

#### Data availability

Data will be made available on request.

#### Acknowledgements

This work was supported by the Czech Science Foundation GA ČR, grant no. 23-06285S and by Czech Ministry of Education, Youth and Sports grant no. CZ.02.01.01/00/22\_008/0004617 – "Energy conversion and storage".

#### References

- [1] Y.R. Golive, A. Kottanharayil, J. Vasi, N. Shiradkar, Determining the optimal standard test condition correction procedure for high-throughput field I-V measurements of photovoltaic modules, *Prog. Photovoltaics Res. Appl.* 30 (2022) 13–26.
- [2] O. Coddington, J. Lean, P. Pilewskie, M. Snow, E. Richard, G. Kopp, C. Lindholm, M. DeLand, S. Marchenko, M. Haberreiter, Solar irradiance variability: comparisons of models and measurements, *Earth Space Sci.* 6 (2019) 2525–2555.
- [3] B. Lipovsek, M. Jost, S. Tomšić, M. Topic, Energy yield of perovskite solar cells: influence of location, orientation, and external light management, *Sol. Energy Mater. Sol. Cell.* 234 (2022) 111421.
- [4] I.M. Peters, T. Buonassisi, How changes in worldwide operating conditions affect solar cell performance, *Sol. Energy* 220 (2021) 671–679.
- [5] A. Srinivasa, J. Karas, A. Augusto, S.G. Bowden, Performance of silicon heterojunction solar cells under low illumination conditions, in: 2018 IEEE 7th World Conference on Photovoltaic Energy Conversion (WCPEC)(A Joint Conference of 45th IEEE PVSC, 28th PVSEC & 34th EU PVSEC), IEEE, 2018, pp. 2070–2073.
- [6] H. Lin, M. Yang, X. Ru, G. Wang, S. Yin, F. Peng, C. Hong, M. Qu, J. Lu, L. Fang, Silicon heterojunction solar cells with up to 26.81% efficiency achieved by electrically optimized nanocrystalline-silicon hole contact layers, *Nat. Energy* 8 (2023) 789–799.
- [7] Q. Su, H. Lin, G. Wang, H. Tang, C. Xue, Z. Li, X. Xu, P. Gao, Theoretical limiting-efficiency assessment on advanced crystalline silicon solar cells with Auger ideality factor and wafer thickness modifications, *Prog. Photovoltaics Res. Appl.* (2024).
- [8] P. Gao, H. Lin, G. Wang, Q. Su, C. Han, C. Xue, S. Yin, L. Fang, X. Xu, Unveiling the Mechanism of Attaining High Fill Factor in Silicon Solar Cells, *Authorea Preprints*, 2023.
- [9] G.E. Bunea, K.E. Wilson, Y. Meydbray, M.P. Campbell, D.M. De Ceuster, Low light performance of mono-crystalline silicon solar cells, in: 2006 IEEE 4th World Conference on Photovoltaic Energy Conference, IEEE, 2006, pp. 1312–1314.
- [10] G. Kim, J.W. Lim, J. Kim, S.J. Yun, M.A. Park, Transparent thin-film silicon solar cells for indoor light harvesting with conversion efficiencies of 36% without photodegradation, *ACS Appl. Mater. Interfaces* 12 (2020) 27122–27130.
- [11] M. Li, F. Igbari, Z.K. Wang, L.S. Liao, Indoor thin-film photovoltaics: progress and challenges, *Adv. Energy Mater.* 10 (2020) 2000641.
- [12] A. Virtuanen, E. Lotter, M. Powalla, U. Rau, J.H. Werner, Highly resistive Cu (In, Ga) Se<sub>2</sub> absorbers for improved low-irradiance performance of thin-film solar cells, *Thin Solid Films* 451 (2004) 160–165.
- [13] S.M. Ahsan, H.A. Khan, Performance comparison of CdTe thin film modules with c-Si modules under low irradiance, *IET Renew. Power Gener.* 13 (2019) 1920–1926.
- [14] K. Shen, Q. Li, D. Wang, R. Yang, Y. Deng, M.-J. Jeng, D. Wang, CdTe solar cell performance under low-intensity light irradiance, *Sol. Energy Mater. Sol. Cell.* 144 (2016) 472–480.
- [15] A.S. Teran, E. Moon, W. Lim, G. Kim, I. Lee, D. Blaauw, J.D. Phillips, Energy harvesting for GaAs photovoltaics under low-flux indoor lighting conditions, *IEEE Trans. Electron. Dev.* 63 (2016) 2820–2825.
- [16] H.K.H. Lee, J. Wu, J. Barbé, S.M. Jain, S. Wood, E.M. Speller, Z. Li, F.A. Castro, J. R. Durrant, W.C. Tsoi, Organic photovoltaic cells—promising indoor light harvesters for self-sustainable electronics, *J. Mater. Chem. A* 6 (2018) 5618–5626.
- [17] Y. Cui, Y. Wang, J. Bergqvist, H. Yao, Y. Xu, B. Gao, C. Yang, S. Zhang, O. Inganäs, F. Gao, Wide-gap non-fullerene acceptor enabling high-performance organic photovoltaic cells for indoor applications, *Nat. Energy* 4 (2019) 768–775.
- [18] S. Braun, G. Micard, G. Hahn, Multi-busbar solar cells and modules: high efficiencies and low silver consumption, *Energy Proc.* 38 (2013) 334–339.
- [19] S. Braun, G. Micard, G. Hahn, Solar cell improvement by using a multi busbar design as front electrode, *Energy Proc.* 27 (2012) 227–233.
- [20] U. Chime, L. Wolf, V. Buga, D. Weigand, A. Gad, J. Köhler, A. Lambertz, W. Duan, K. Ding, T. Merdzhanova, How thin practical silicon heterojunction solar cells could Be? Experimental study under 1 sun and under indoor illumination, *Sol. RRL* 6 (2022) 2100594.
- [21] J. Cattin, O. Dupré, B. Aïssa, J. Haschke, C. Ballif, M. Boccard, Optimized design of silicon heterojunction solar cells for field operating conditions, *IEEE J. Photovoltaics* 9 (2019) 1541–1547.
- [22] B. Conrad, L. Antognini, A.P. Amalathas, M. Boccard, J. Holovský, Illumination-dependent requirements for heterojunctions and carrier-selective contacts on silicon, *IEEE J. Photovoltaics* 10 (2020) 1214–1225.

- [23] R.K. Sharma, M. Boccard, J. Holovský, New metric for carrier selective contacts for silicon heterojunction solar cells, *Sol. Energy* 244 (2022) 168–174.
- [24] R. Lachaume, W. Favre, P. Scheiblin, X. Garros, N. Nguyen, J. Coignus, D. Munoz, G. Reimbold, Influence of a-Si:H/TTO interface properties on performance of heterojunction solar cells, *Energy Proc.* 38 (2013) 770–776.
- [25] I. Silvaco, ATLAS User's Manual, 2011, p. 5. Santa Clara, CA, Ver.
- [26] B. Kuhlmann, A.G. Aberle, R. Hezel, G. Heiser, Simulation and optimization of metal-insulator-semiconductor inversion-layer silicon solar cells, *IEEE Trans. Electron. Dev.* 47 (2000) 2167–2178.